ACS APPLIED ENERGY MATERIALS

www.acsaem.org Article

4.9% Efficient Sb_2S_3 Solar Cells from Semitransparent Absorbers with Fluorene-Based Thiophene-Terminated Hole Conductors

Sreekanth Mandati,* Nimish Juneja, Atanas Katerski, Aistė Jegorovė, Raitis Grzibovskis, Aivars Vembris, Tatjana Dedova, Nicolae Spalatu, Artiom Magomedov, Smagul Karazhanov, Vytautas Getautis, Malle Krunks, and Ilona Oja Acik*

Cite This: *ACS Appl. Energy Mater.* 2023, 6, 3822−3833 Read Online

ACCESS | Metrics & More | Article Recommendations | Supporting Information

ABSTRACT: Fluorene-based hole transport materials (HTMs) with terminating thiophene units are explored, for the first time, for antimony sulfide (Sb_2S_3) solar cells. These HTMs possess largely simplified synthesis processes and high yields compared to the conventional expensive hole conductors making them reasonably economical. The thiophene unit-linked HTMs have been successfully demonstrated in ultrasonic spray-deposited Sb_2S_3 solar cells resulting in efficiencies in the range of 4.7−4.9% with an average visible transmittance (AVT) of 30−33% (400−800 nm) for the cell stack without metal contact, while the cells fabricated using conventional P3HT have yielded an efficiency of 4.7% with an AVT of 26%. The study puts forward cost-effective and transparent HTMs that avoid a post-coating activation at elevated temperatures like P3HT, devoid of parasitic absorption losses in the visible region and are demonstrated to be well aligned for the band edges of Sb_2S_3 thereby ascertaining their suitability for Sb_2S_3 solar cells and are potential candidates for semitransparent applications.

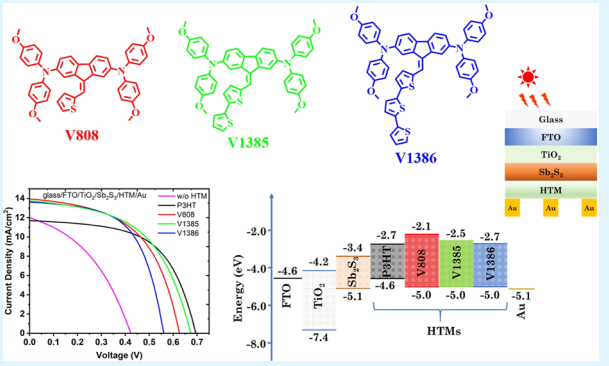

KEYWORDS: *antimony sulfide, solar cells, thiophene, hole transport material, semitransparent*

1. INTRODUCTION

The energy crisis is among the major problems of the present day's growing world with digitalization and the internet of things. In addition, the limited availability of fossil fuels, the dominant sources of current days' energy and the associated problems of pollutant emissions by burning fossil fuels is a bigger concern. Considering the UNO's policies of net-zero emissions by 2050 coupled with the goals set by many countries worldwide to produce clean energy necessitates the requirement of alternative energy sources that are clean, abundant, and easy to harvest. Renewable energy technologies are the need of the hour to meet these demands and among them, solar photovoltaics (PV) is a technology that has tremendous potential to be a major yet important energy harvesting source. Solar energy is abundantly available and PV is a green technology that facilitates the conversion of sunlight to electricity in a clean manner once the solar panels are in fully operational condition. Furthermore, building-integrated photovoltaics (BIPV) is an emerging technology in PV wherein solar panels could be integrated into buildings that produce energy to meet some portion of energy demand within. Energy-efficient buildings are going to be the future with the growing smart city infrastructure and contribute effectively toward net-zero emissions. Semitransparent solar cells could play an important role in BIPV and could be integrated into windows. Intense investigations are underway to explore novel materials and device architectures that are suitable for semitransparent solar cells.

Among various emerging materials, antimony sulfide (Sb_2S_3) is the promising candidate for the photovoltaic community owing to the earth-abundant and environmentally friendly constituent elements alongside appropriate optoelectronic properties such as a desirable band gap of ≈1.7 eV, large absorption coefficient (≈10^5 cm^{-1}) and long-term stability.[1−3] The Shockley−Queisser limit of the power conversion efficiency (PCE) of the single junction Sb_2S_3 solar cells is 28.64%.[1] Sb_2S_3 absorbers are potential contenders for semitransparent solar cells due to their relatively wide band gap and the possibility to yield higher PCEs even with very thin absorber layers (≈100 nm).[4] Further, the wide band gap of Sb_2S_3 also makes them a wiser choice for tandem cell applications.[5−7] The highest reported PCE of Sb_2S_3 solar cells

Received: December 21, 2022
Accepted: March 14, 2023
Published: March 23, 2023

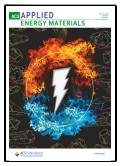

Table 1. Reported Device Parameters of Sb_2S_3 Solar Cells with Different HTMs, Device Configurations, Methods of Preparation, and Thicknesses[a]

HTM	device configuration	Sb_2S_3(deposition technique)	Sb_2S_3thickness (nm)	solar cell parameters				reference
				V_{OC} (mV)	J_{SC} (mA/cm^2)	FF (%)	PCE (%)	
P3HT	ITO/ZnO/Sb_2S_3/P3HT/Ag	TE	210	450	12.6	42	2.4	21
	ITO/TiO_2/Sb_2S_3/P3HT/Au	CBD	200	630	6.1	35	1.4	22
	ITO/TiO_2/Sb_2S_3/P3HT/Ag	ALD	155	732	9.3	62	4.3	2
	FTO/TiO_2/Sb_2S_3/P3HT/Au	SC		616	8.1	46	2.3	16
	ITO/TiO_2/Sb_2S_3/P3HT/Au	USP	150	618	6.0	51	1.9	23
	ITO/TiO_2/Sb_2S_3/P3HT/Au	USP	100	693	13.8	58	5.5	6
Spiro-OMeTAD	FTO/TiO_2/Sb_2S_3/Spiro-OMeTAD/Au	CBD	84	690	13.4	50	4.6	17
	FTO/TiO_2/Sb_2S_3/Spiro-OMeTAD/Au	SC	400	660	13.1	59	5.2	18
	FTO/TiO_2/Sb_2S_3/Spiro-OMeTAD/Au	SC	140	632	12.9	52	4.3	24
	FTO/TiO_2/Sb_2S_3/Spiro-OMeTAD/Ag	TE	300	620	10.7	56	3.8	25
	FTO/TiO_2/Sb_2S_3/Spiro-OMeTAD/Au	SC	162	650	17.7	62	7.1	26
	FTO/TiO_2/Sb_2S_3/Spiro-OMeTAD/Au	SC	146	720	17.2	57	7.1	27
	FTO/CdS/Sb_2S_3/Spiro-OMeTAD/Au	HT	300	707	15.2	56	6.0	28
	FTO/CdS/Sb_2S_3/Spiro-OMeTAD/Au	TE	200	720	15.9	54	6.2	29
	FTO/TiO_2/CdS/Sb_2S_3/Spiro-OMeTAD/Au	HT	1000	748	15.3	57	6.5	30
	FTO/CdS/Sb_2S_3/Spiro-OMeTAD/Au	CBD	214	757	17.4	60.5	8.0	8
P3HT/PEDOT:PSS	FTO/TiO_2/ZnS/Sb_2S_3/P3HT/PEDOT:PSS/Au	ALD	75	626	15.7	52	5.1	31
	FTO/TiO_2/Sb_2S_3/P3HT/PEDOT:PSS/Au	ALD	90	667	14.9	58	5.8	32
V1236	FTO/TiO_2/Sb_2S_3/HTM/Au	USP	90	612	13.8	46	3.9	33

[a]HTM: hole transport material; TE: thermal evaporation; CBD: chemical bath deposition; SC: spin coating; USP: ultrasonic spray pyrolysis; HT: hydrothermal; ALD: atomic layer deposition, V1236: (N^2,N^2,N^7,N^7-tetrakis[2,2-bis(4-methoxyphenyl)vinyl]-9,9-dihexyl-9*H*-fluorene-2,7-diamine).

is 8%, achieved recently through a multi-sulfur source approach using the chemical bath deposition method (CBD).[8] The overall efficiencies are rather limited by the deficiencies in open circuit voltage (V_{OC}) that are attributed to the self-trapping of carriers due to lattice deformation and/or to the intrinsic defects, which sets the maximum attainable V_{OC} to 0.8 V.[9,10] Antimony selenide (Sb_2Se_3), another class of antimony chalcogenide, is also a potential candidate for PV applications and is explored extensively.[11−13]

In addition to the considerable challenges in improving the PCEs, the method of Sb_2S_3 absorber fabrication is critical for upscaling. The high-efficiency Sb_2S_3 solar cells so far are mostly prepared by spin coating and CBD.[8−15] While the spin coating technique demonstrates excellent control of parameters and reproducibility but is limited to laboratory scale and also has high material wastage (>90%). CBD, on the other hand, has promise for large-scale demonstration but needs longer deposition time at relatively low temperatures (<10 °C) to obtain the desired thickness of the absorbers. Our group has previously demonstrated the fabrication of Sb_2S_3 solar cells by the ultrasonic spray pyrolysis method, which offers large-area uniformity and is an industrially scalable technique with low capital.[6] Further, the Sb_2S_3 solar cells are often fabricated in planar superstrate configuration wherein TiO_2 is the most commonly used electron transport layer (ETL) deposited on a transparent conducting oxide followed by the Sb_2S_3 absorber, hole transport material (HTM), and finally, the back contact, often Au. HTMs are the vital component of planar or mesoscopic Sb_2S_3 solar cells that drive the transport of photogenerated holes to the back contact and reduce recombination losses.[2] In general, conventional HTMs like poly(3-hexylthiophene) (P3HT),[2,16] 2,2′,7,7′-tetrakis[*N*,*N*-di(4-methoxyphenyl)amino]-9,9′-spirobifluorene (Spiro-OMeTAD),[17,18] poly{4,4-dialkyl-4*H*-cyclopenta[2,1-*b*;3,4-*b*′]-dithiophene-2,6-diyl-*alt*-2,1,3-benzothiadiazole-4,7-diyl} (PCPDTBT),[19,20] etc. are the most commonly employed in the fabrication of Sb_2S_3 solar cells. The use of these different HTMs in Sb_2S_3 solar cells where the Sb_2S_3 absorbers are prepared by different techniques and device architectures are summarized in Table 1 alongside the power conversion efficiencies achieved. It may be noted that only organic HTMs and planar configuration devices are considered for summary.

It may be noted that except for V1236, an economic and transparent hole conductor previously reported by our group,[33] other studies have majorly used conventional P3HT and Spiro-OMeTAD. These hole conductors are very expensive mainly due to their complex, expensive, and time-consuming synthesis processes[34] and are also moisture sensitive, and thereby could be significant barriers to the potential upscale for commercial applications. Further, tailoring HTMs with suitable thickness is also important to obtain high-efficiency solar cells but may hinder the overall transparency of the solar cell stack, an important parameter in semitransparent solar cells. For instance, the commonly employed P3HT exhibits parasitic absorption in the visible spectral region, which induces a loss in the total transmittance of the solar cell.[2,33] In addition, P3HT also requires additional post-coating activation at temperatures around 170 °C either in a vacuum or inert atmosphere.[35] Therefore, it becomes imperative to explore low-cost novel HTMs, which could be easily synthesized using available commercial starting materials while possessing suitable properties like good thermal stability, desired solubility, and hole mobility.

In view of the above, the study herein proposes to fabricate Sb_2S_3 solar cells by a scalable and industrially benign ultrasonic

https://doi.org/10.1021/acsaem.2c04097
ACS Appl. Energy Mater. 2023, 6, 3822−3833

spray pyrolysis (USP) method by employing novel, low-cost, and transparent hole conductors from fluorene-based molecules with terminated thiophene units. The 4,4′-dimethoxydiphenylamine-substituted fluorene fragment is used due to its wider application in the organic HTMs, in particular, Spiro-OMeTAD, while thiophene units are added mimicking P3HT HTM. The new materials follow simple synthesis processes with high yields thereby having considerably lower costs than conventional HTMs. Sb_2S_3 solar cells with new HTMs are fabricated in the standard superstrate configuration wherein ETL and absorber are deposited by USP while HTMs are spin coated followed by the thermal evaporation of Au. Comprehensive characterization of solar cells through different techniques clearly demonstrates that the cells with new HTMs yield similar or better PCEs compared to the conventional P3HT-based devices and have exhibited enhanced average visible transmittance in the 400−800 nm range. Further, the band energetics show that the new HTMs possess favorable band alignment with the Sb_2S_3 absorber thereby validating their efficacy toward semitransparent solar cells.

Scheme 1. Synthetic Route to the Novel Hole Transporting Materials V808, V1385, and V1386

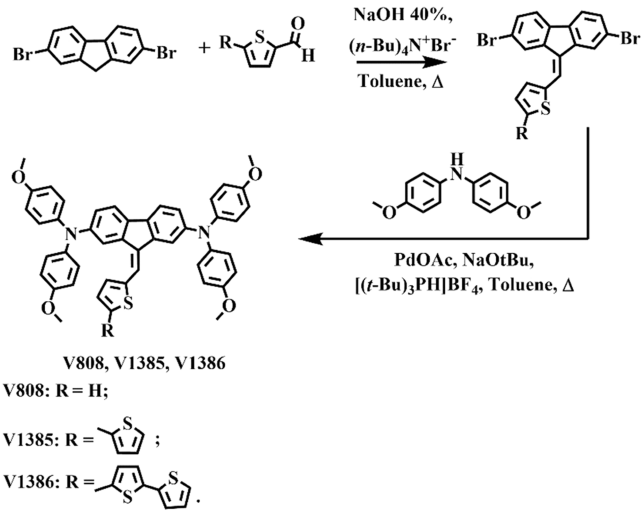

V808, V1385, V1386

V808: R = H;

V1385: R = ;

V1386: R = .

2. EXPERIMENTAL SECTION

2.1. Materials. The following materials were used: FTO substrate (7 Ω sq^{-1}), titanium(IV) tetraisopropoxide (TTIP)—99 wt % (Acros Organics), acetylacetone—99 wt % (Acros Organics), ethanol—96.6 vol % (Estonian Spirit), methanol—99.9 vol % (Sigma-Aldrich), antimony trichloride—99.99 wt % (Sigma-Aldrich), thiourea—99 wt % (Sigma-Aldrich), chlorobenzene—99.5 vol % (Sigma-Aldrich), poly(3-hexyl-thiophene-2,5-diyl) (P3HT)—100 kDa, >90% regioregular (Sigma-Aldrich), and materials related to HTM synthesis as mentioned in the S1. The materials were used as received.

2.2. Solar Cell Fabrication. Antimony sulfide (Sb_2S_3) solar cells were fabricated in superstrate configuration (glass/FTO/TiO_2/Sb_2S_3/HTM/Au). The fabrication process started with thorough cleaning of the glass/FTO substrate with DI water, acetone, and IPA in an ultrasonic bath for 10 min each followed by boiling the substrates in DI water and purging with N_2 gas. The TiO_2 electron transport layer (ETL) and Sb_2S_3 absorbers were deposited by an indigenously made ultrasonic spray deposition system. TiO_2 was sprayed from a solution mixture of 0.2 M TTIP with 0.2 M acetylacetone in ethanol by using a spray rate of ≈2.5 mL/min for 30 min on a hot plate maintained at around 340 °C. The sprayed TiO_2 samples were then annealed at 450 °C for 30 min in air. Sb_2S_3 thin films were spray-deposited from a solution mixture of 60 mM $SbCl_3$ and 180 mM thiourea in methanol. The films were deposited at a spray rate of 2 mL/min while maintaining a substrate temperature of ≈200 °C. The as-deposited Sb_2S_3 films were annealed at around 250−260 °C for 5 min under nitrogen. The hole transport materials (HTM) explored in this study are the fluorene-based molecules with linked thiophene units N^2,N^2,N^7,N^7-tetrakis(4-methoxyphenyl)-9-(thiophen-2-ylmethylene)-9*H*-fluorene-2,7-diamine (**V808**), 9-([2,2′:5′,2″-terthiophen]-5-yl-methylene)-N^2,N^2,N^7,N^7-tetrakis(4-methoxyphenyl)-9*H*-fluorene-2,7-diamine (**V1385**), and 9-([2,2′-bithiophen]-5-ylmethylene)-N^2,N^2,N^7,N^7-tetrakis(4-methoxyphenyl)-9*H*-fluorene-2,7-diamine (**V1386**). The detailed synthesis procedure of **V808**, **V1385**, and **V1386** is described in Section S1 while the synthesis process is presented in Scheme 1. The HTM layers were spin coated on glass/FTO/TiO_2/Sb_2S_3 samples followed by the thermal evaporation of Au contacts. The active area of solar cells was 7.06 mm^2.

2.3. Characterization. The crystal structure and phase constitution of the as-deposited and annealed Sb_2S_3 thin films were examined using a Rigaku Ultima IV X-ray diffractometer with a Cu Kα source (λ = 1.5406 Å). In addition, micro-Raman spectroscopy was further used to ascertain the crystalline purity while also detecting the possible presence of the minute antimony oxide phase and micro-Raman spectra were recorded at room temperature using a Horiba Labram HR 800 in backscattering mode with a He Ne laser of 532 nm. A Zeiss HR FESEM was used to analyze the cross-sectional morphologies of the layers. The optical absorption and transmittance measurements were made using a Jasco V-670 ultraviolet−visible spectrophotometer (UV−VIS) in the range of 300−1000 nm. For the band diagram construction, photoelectron emission spectroscopy (PES) and photoconductivity methods were used. For these methods, the measurement system consisted of an ENERGETIQ Laser-Driven Light Source (LDLS EQ-99) as a light source, a Spectral Products DK240 1/4m monochromator, and a Keithley 617 electrometer. The measurements were performed in vacuum at a pressure of ∼10^{-5} mbar. Both methods are described in detail in S2. The hole transport materials were characterized comprehensively using thermogravimetric analysis (TGA), differential scanning calorimetric (DSC) analysis, and absorption spectroscopy. The work function of Au contacts was measured using a Kelvin probe. The current−voltage (I−V) characteristics of the fabricated solar cells were measured using Wavelabs LS-2 LED solar simulator with an AM1.5G (100 mW cm^{-2}) light source. A Newport 69911 system with a 300 W Xenon lamp was used to measure the external quantum efficiency (EQE) of the fabricated solar cells.

3. RESULTS AND DISCUSSION

The fluorene-based thiophene-linked hole transport materials (HTMs) are explored in this study for the fabrication of Sb_2S_3 solar cells. The design of these p-type photoconductors has been inspired by recently published findings that thiophene can coordinate with Sb atoms in $Sb_2(S,Se)_3$ leading to the improvement of the interfacial properties between $Sb_2(S,Se)_3$ and HTM.[36,37] This interaction provides desirable channels for carrier transport, which significantly enhances the open circuit voltage and fill factor. In a single thiophene unit-linked molecule (**V808**), 4,4-dimethoxydiphenylamine chromophores are symmetrically connected on both sides of the fluorene core, which was easily modified chemically by the thiophene end-group. **V808** is synthesized through a simple two-step process (Scheme 1) devoid of expensive/complex materials/steps with considerably good yields thereby resulting in low synthesis costs. On a similar note, to further investigate the possibility of better interaction, the molecules are synthesized by adding 2 and 3 thiophene units to the fluorene core, which are thus named **V1385** and **V1386**, respectively. The detailed synthesis procedure of **V808**, **V1385**, and **V1386** is described in Section S1 and the cost estimation is given in Tables S1−S3, respectively. It may be observed that the synthesis cost of a

https://doi.org/10.1021/acsaem.2c04097
ACS Appl. Energy Mater. 2023, 6, 3822−3833

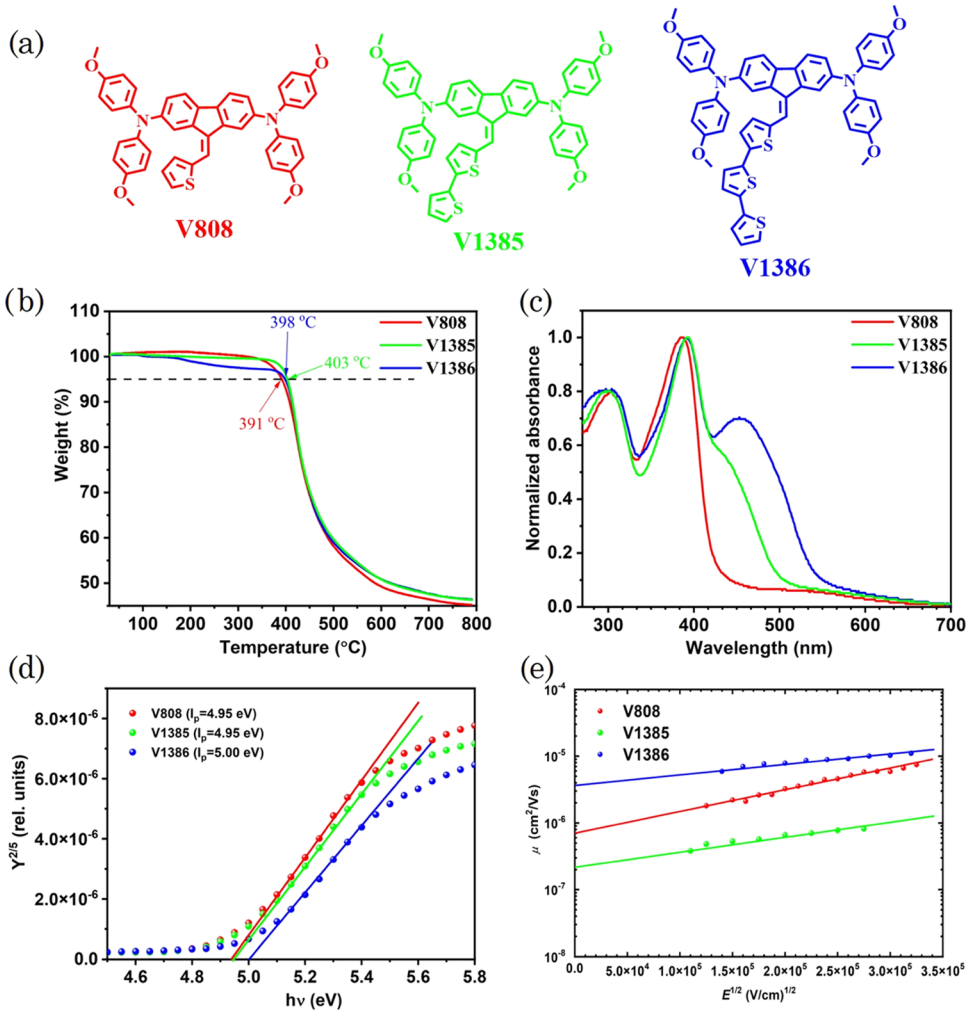

Figure 1. (a) Chemical structures of new fluorene-based hole transport materials with terminating thiophene units (**V808**, **V1385**, and **V1386**), (b) thermogravimetric analysis (TGA) data, (c) normalized absorbance spectra of the HTMs deposited on glass, (d) photoemission spectra in air for determining the ionization potential, and (e) electric field dependencies of the hole mobility of **V808**, **V1385**, and **V1386**.

single thiophene linking molecule (**V808**) is ≈13 € per gram while those of the ones with 2 and 3 thiophene units are 32 and 177 € per gram, respectively, indicating the increase in cost is majorly owing to the increased price of the starting thiophenecarbaldehyde. However, the cost of single and double thiophene unit-linked molecules (**V808** and **V1385**) is considerably cheaper in comparison to the conventional hole conductors like P3HT and Spiro-OMeTAD. Irrespective of the cost, all three materials are comprehensively characterized and are explored as HTMs in Sb_2S_3 solar cells. The typical chemical structures of **V808**, **V1385**, and **V1386** with 1, 2, and 3 linked thiophene units, respectively, are shown in Figure 1a. Figure 1b shows the thermogravimetric analysis (TGA) curves of **V808**, **V1385**, and **V1386**, and as the plots reveal all three materials start to decompose at temperatures >390 °C, which is far above the temperature for conventional device operation. The differential scanning calorimetric (DSC) curves of new HTMs are shown in Figure S1. All compounds have shown T_g slightly less than 100 °C (92, 97, and 99 °C for **V808, V1385**, and **V1386**, respectively). Comparison of T_g of new materials reveals that an increase in thiophene fragments in the molecule leads to slightly increased T_g, and could be attributed to the increased molecular weight. In addition, it is important to note that the melting process is observed just for **V808**, while other new synthesized compounds (**V1385** and **V1386**) have shown no endothermic peaks, indicating that they have only an amorphous state, which is an advantage for the formation of homogenous films as it eliminates the possibility of crystallization of films during preparation/operation of devices. The normalized absorbance spectra of the films, deposited on glass, are shown in Figure 1c. As can be seen, the spectra of new compounds display intensive $\pi-\pi^*$ absorption bands at 270−430 nm, which might be attributed to the 4,4′-dimethoxydiphenylamine-substituted fluorene fragment. In addition, with the increase in the number of thiophene units, the ($\pi-\pi^*$) transition associated with this conjugated part exhibits a strong bathochromic shift. For compound **V1386**, this results in a band with the absorption maximum at 453 nm, for **V1385** it appears as a shoulder to the main peak, while for **V808** it overlaps with the main peak. The normalized absorbance spectra of new HTMs are also compared with the conventional P3HT as presented in Figure S2, which shows that P3HT absorbs significantly in the 400−650 nm region while the new HTMs possess much less absorption in the same region thereby demonstrating better visible light transparency.

The solid-state ionization potential (I_p) of HTMs is determined using photoelectron emission spectroscopy

https://doi.org/10.1021/acsaem.2c04097
ACS Appl. Energy Mater. 2023, 6, 3822−3833

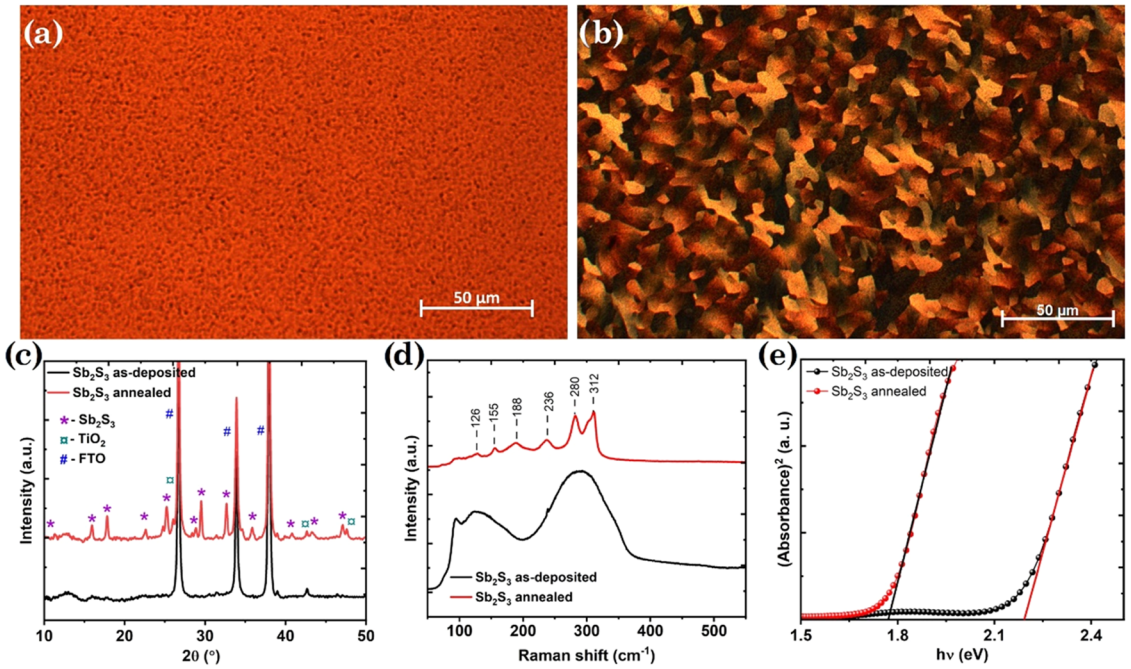

Figure 2. Morphological, structural, and optical characteristics of Sb_2S_3 thin films deposited by ultrasonic spray pyrolysis: Optical microscopy images of (a) as-deposited and (b) annealed Sb_2S_3, (c) XRD patterns, (d) Raman spectra, and (e) $(\text{absorbance})^2$ vs $h\nu$ plots of as-deposited and annealed Sb_2S_3.

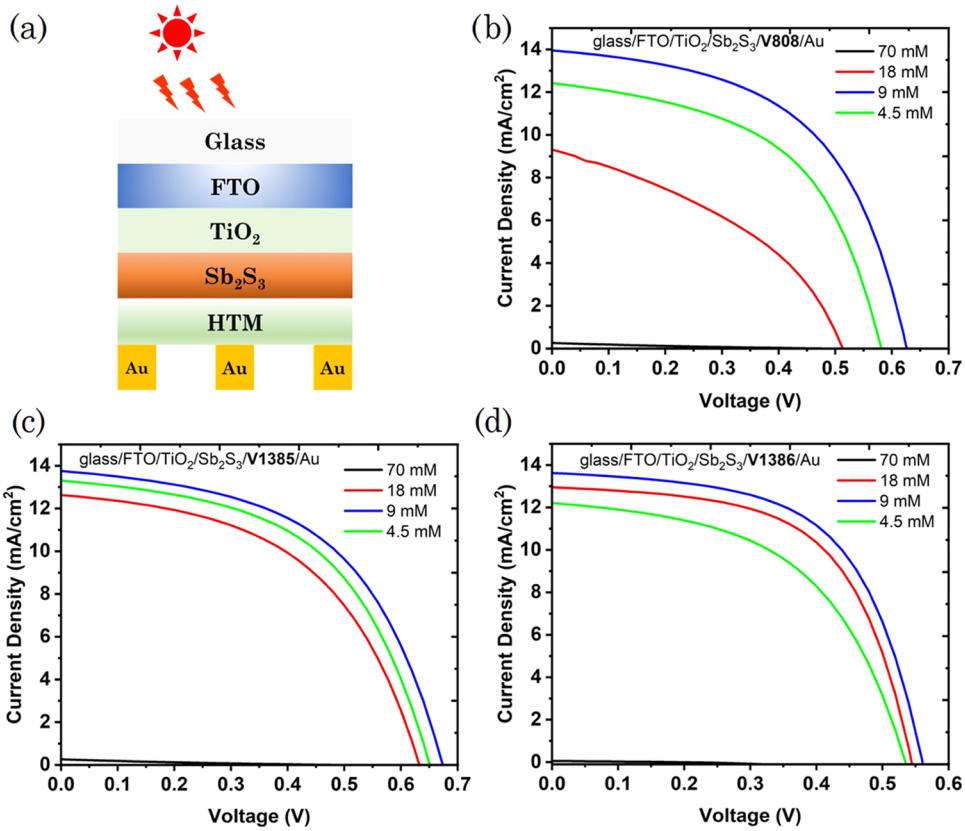

Figure 3. (a) Schematic illustration of device configuration (glass/FTO/TiO_2/Sb_2S_3/HTM/Au) of Sb_2S_3 solar cells (Note: Not to scale), $J-V$ characteristics of solar cells with (b) **V808**, (c) **V1385**, and (d) **V1386** as HTMs with the variation in precursor concentrations from 4.5 to 70 mM in each case.

(PES) of the thin films (Figure 1d), which clearly reveals that the I_p levels of **V808**, **V1385**, and **V1386** are determined to be −4.95 eV, −4.95, and −5.00 eV, respectively. Almost similar I_p values can be explained by the unfavorable arrangement of thiophene fragments. As can be seen from absorbance spectra, the increase of the conjugated system is very slight with the

https://doi.org/10.1021/acsaem.2c04097
ACS Appl. Energy Mater. 2023, 6, 3822−3833

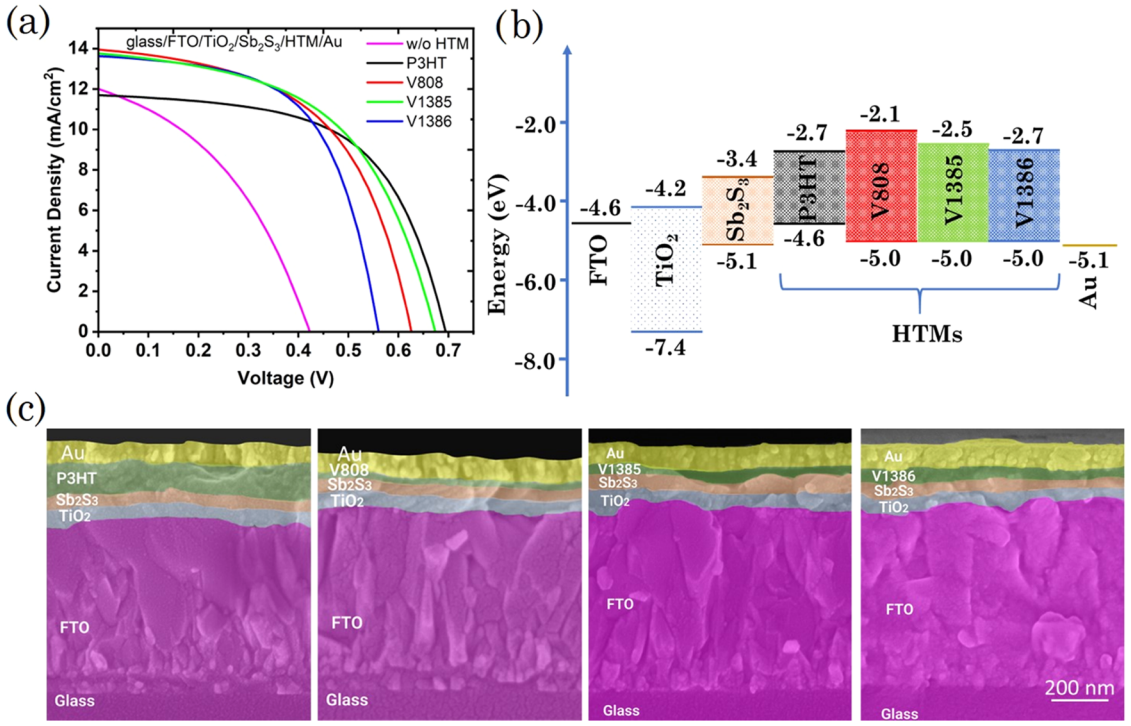

Figure 4. (a) $J-V$ characteristics of champion cells, (b) band energy diagram and (c) cross-sectional images of Sb_2S_3 solar cells with P3HT, **V808**, **V1385**, and **V1386** as HTMs, respectively.

increasing number of thiophene moieties in the molecule, therefore the highest occupied molecular orbital (HOMO) levels can be very similar. Further, hole drift-mobility of HTMs is estimated using the time of flight (ToF) method with Ekspla PL kHz ps tunable laser as a light source and a Tektronix MDO3024 oscilloscope for signal registration. As shown in Figure 1e, the inferred zero-field hole mobilities are 7.07×10^{-7}, 2.15×10^{-7}, and 3.68×10^{-6} $cm^2/(V{\cdot}s)$, for **V808**, **V1385**, and **V1386**, respectively.

Sb_2S_3 thin films are deposited by the USP process on glass/FTO/TiO_2 samples. Optical microscopic images are recorded to ascertain the conformal coverage of Sb_2S_3 films on TiO_2 as shown in Figure 2a and as the image, which is recorded for a considerably larger area, unveils that the films are conformally covered devoid of any pin holes or crystallization during the deposition. The crystallization of Sb_2S_3 thin films during deposition in the USP process is a commonly observed feature, which is a detrimental process that reduces the quality of films for solar cell applications as this crystallization during deposition is an uncontrollable process and the resulting crystallinity is not the desired form too, which is absent in the present study. Further, the as-deposited films are characterized by XRD and Raman as shown in Figure 2c,d. The XRD pattern shows the sharp peaks pertaining to FTO and TiO_2 layers while the Raman spectra reveal broad characteristic peaks of Sb_2S_3 confirming that the as-deposited films are amorphous in nature. Upon annealing under a nitrogen atmosphere at 250 °C, the Sb_2S_3 films exhibit crystallinity. Optical microscopy images of annealed Sb_2S_3 films show a large grain structure as shown in Figure 2b without any voids or pin holes. The XRD patterns of annealed Sb_2S_3 show several sharp peaks in addition to the existing FTO and TiO_2 peaks, which correspond to the orthorhombic stibnite Sb_2S_3 phase (ICDD PDF 01-075-4013). On a similar note, the Raman spectra of annealed Sb_2S_3 show sharp peaks characteristic of Sb_2S_3 thereby corroborating the XRD analysis and confirming the formation of the crystalline stibnite Sb_2S_3 phase. Further, the band gap of Sb_2S_3 absorbers is inferred from $(\text{absorbance})^2$ vs $h\nu$ plots as shown in Figure 2e. The band gap of amorphous Sb_2S_3 is determined to be around 2.2 eV while that of crystallized one is 1.7 eV, which agree well with the values reported previously.[33] Therefore, it may be inferred that the crystalline Sb_2S_3 absorbers with the desired band gap are successfully fabricated by the area-scalable USP process followed by annealing.

In the next step, the Sb_2S_3 solar cells are fabricated in the planar configuration, as shown in Figure 3a, using conventional P3HT and new **V808**, **V1385**, and **V1386** as HTMs, which are spin coated onto glass/FTO/TiO_2/Sb_2S_3 samples and Au is thermally evaporated. While the concentration of P3HT has been previously optimized for the best efficient Sb_2S_3 solar cells,[33] the new HTMs require a similar process. Therefore, prior to comparison with P3HT-based solar cells, the concentration of the precursors in spin coating has been optimized for new HTMs. Figure 3b–d shows the current density–voltage ($J-V$) characteristics of solar cells with concentration variation in each case for **V808**, **V1385**, and **V1386**, respectively. The variation in the associated device parameters with concentration is shown in Figure S3. For an initial concentration of 70 mM **V808**, the solar cells exhibit very low PCEs, essentially due to the negligible photocurrent. The concentration of **V808** is therefore diluted considerably in steps of ca. 4× resulting in 18, 9, and 4.5 mM. As shown in the $J-V$ curves in Figure 3b, the efficiencies of solar cells for **V808** concentrations of 70, 18, 9, and 4.5 mM are 0.1, 2.0, 4.7, and 3.8%, respectively. The device parameters, V_{OC}, J_{SC}, and FF have followed an identical trend that the respective values are maximum for 9 mM **V808** and are lower on either side (see Figure S3a,b). To identify the plausible reasons, the series resistance (R_s) of the devices is determined from the $J-V$ data

https://doi.org/10.1021/acsaem.2c04097
ACS Appl. Energy Mater. 2023, 6, 3822–3833

that a very large R_s (>200 Ω·cm^2) is observed for the 70 mM **V808** device, which decreased significantly with a decrease in the concentration resulting in considerable improvement in J_{SC}. The large R_s may be attributed to the larger thickness of **V808** arising from the large concentration. It may therefore be concluded that 9 mM **V808** is considered optimal resulting in the highest PCE among all. On a similar note, the power conversion efficiencies of the solar cells with 70, 18, 9, and 4.5 mM concentrations of **V1385** are obtained to be 0.2, 4.0, 4.9, and 4.5%, respectively. For the case of **V1386**, the obtained efficiencies are 0.15, 4.1, 4.5, and 3.4% for concentrations of 70, 18, 9, and 4.5 mM. The variation trends in the associated device parameters are also similar as shown in Figure S3c−f. It may therefore be inferred that the 9 mM concentration in each case has resulted in the best device efficiencies of 4.7, 4.9, and 4.5% for solar cells with **V808**, **V1385**, and **V1386** as HTMs, respectively.

While the new molecules **V808**, **V1385**, and **V1386** have demonstrated reasonable efficiencies, it is important to compare them with existing conventional proven HTMs. Therefore, to further validate the efficacy of new molecules as the HTM layer in Sb_2S_3 solar cells, they are compared with conventional P3HT-based devices. The $J-V$ characteristics of champion Sb_2S_3 solar cells with P3HT, **V808**, **V1385**, and **V1386** are shown in Figure 4a. In addition, to understand the need for an HTM in devices, solar cells fabricated without the HTM layer are also shown. The device parameters are listed in Table 2. The solar cells without HTM have exhibited a PCE of

Table 2. Device Parameters of Champion Sb_2S_3 Solar Cells with P3HT, V808, V1385, and V1386 HTMs

HTM	V_{OC} (V)	J_{SC} (mA/cm^2)	FF	PCE (%)	R_s (Ω·cm^2)	R_{SH} (Ω·cm^2)
no HTM	0.43	12.0	0.41	2.12	1.33	167
P3HT	0.69	11.7	0.58	4.68	2.1	1190
V808	0.63	13.9	0.54	4.73	1.01	586
V1385	0.68	13.7	0.53	4.94	2.3	569
V1386	0.56	13.6	0.59	4.50	0.89	844

2.12% with a reasonably low V_{OC} of 0.43 V, a J_{SC} of 12.0 mA/cm^2, and an FF of 0.41. Such characteristics are often classically observed for bare Sb_2S_3-based solar cells devoid of HTM. The band energy positions of different device layers explored in the present study are determined using photoelectron emission spectroscopy and the band energy diagram is presented in Figure 4b. The Sb_2S_3 absorber possesses the valence (VBE) and conduction band edges (CBE) at −5.1 and −3.4 eV, respectively, and with Au and TiO_2 on either side of the absorber in solar cells without HTM, the transport of photogenerated electrons and holes is reasonably smooth owing to the favorable band edge positions. However, with Au being the back contact there is no barrier for electrons from the conduction band of Sb_2S_3 at the Sb_2S_3-Au interface thereby leading to recombination often resulting in low V_{OC} and FF. The devices also exhibit a very low shunt resistance (R_{SH}) of ≈167 Ω·cm^2. On the other hand, the solar cells with conventional P3HT have demonstrated a PCE of 4.68% with a V_{OC} of 0.69 V, a J_{SC} of 11.7 mA/cm^2, and an FF of 0.58. It can be observed that the device parameters are considerably increased, particularly the V_{OC} and FF. The presence of an HTM contributes in various ways to enhance the conversion efficiency of solar cells as they improve band energetics of the device for improved transport of photogenerated carriers while reducing recombination losses as they block the electrons by passivating the interface across Sb_2S_3-HTM. As seen from Figure 4b, P3HT possesses the VBE and CBE at −4.6 and −2.7 eV, respectively, that its presence could provide a barrier at the Sb_2S_3−HTM interface for the electrons to travel back and therefore, reduce the recombination losses. The devices have shown a significantly enhanced $R_{SH} \approx 1.2$ kΩ·cm^2, an almost 7-fold increment compared to the bare cells. It may also be observed that the series resistance (R_s) of the P3HT-based devices has slightly increased compared to the bare cells and could be due to the additional P3HT layer, which is a reasonably resistive material. However, due to the enhanced charge transport and reduced recombination losses owing to the favorable band alignment, the V_{OC} is significantly increased and J_{SC} has not changed hugely despite the higher R_s.

The solar cells with new HTMs have demonstrated efficiencies of 4.73, 4.94, and 4.50% for **V808**, **V1385**, and **V1386**, respectively. Primarily, it is important to note that the new HTMs have exhibited efficiencies either on par or slightly higher than the conventional P3HT, which clearly demonstrates their validation. Another major observation from Figure 4a and Table 2 is that the solar cells with **V808**, **V1385**, and **V1386** have yielded considerably higher J_{SC}, almost close to 14 mA/cm^2 over the P3HT devices (11.7 mA/cm^2). However, the V_{OC} values of the devices with new HTMs are relatively lower than that of P3HT devices. As can be seen, the V_{OC} of solar cells with **V808**, **V1385**, and **V1386** are 0.63, 0.68, and 0.56, respectively, while the V_{OC} of P3HT-based solar cells is 0.69 V. The band edge positions of new HTMs are compared with P3HT alongside other device layers as shown in Figure 4b and it can be observed that all the new HTMs possess the same VBE at −5.0 eV while that of P3HT is −4.6 eV. For the transport of photogenerated holes, the VBE of P3HT is in a favorable position with respect to the Sb_2S_3 absorber compared to the new HTMs, however, with the back contact (Au) energy level being −5.1 eV, the relatively smoother transport of holes is feasible in solar cells with new HTMs compared to P3HT. In addition, the CBE positions of new HTMs are −2.1, −2.5, and −2.7 eV for **V808**, **V1385**, and **V1386**, respectively, compared to P3HT (−2.7 eV). As may be observed, the interface barrier at the Sb_2S_3-HTM interface is larger for new HTMs over P3HT, which is responsible for electron blocking at the interface and leads to reduced recombination losses. While the higher J_{SC} may be ascribed to the favorable band alignment of new HTMs, the lower V_{OC} values compared to P3HT are not as expected especially considering the larger band gap of new HTMs than P3HT. Particularly, considerably lower V_{OC} (0.56 V) in solar cells with **V1386** with a deficiency of almost 100 mV or more compared to other solar cells despite its reasonably higher mobility is still a question, although it may be speculated that this is owing to the increase in the number of thiophene units, the coverage might not be as uniform as compared to other layers leading to agglomerated conducting paths that may act as trap centers for photogenerated carriers. On that note, the wettability of new HTMs alongside P3HT in their precursor form is explored on the Sb_2S_3 surface. It is observed that all the HTMs including P3HT have shown excellent wettability with close to 0° contact angle for new HTMs and 2° for P3HT. The visual appearance of the samples upon dropping the precursor droplet onto Sb_2S_3 indicates that the P3HT drop remains as it is while the new HTM precursor drop spreads quickly in no time, which shows the relatively

https://doi.org/10.1021/acsaem.2c04097
ACS Appl. Energy Mater. 2023, 6, 3822−3833

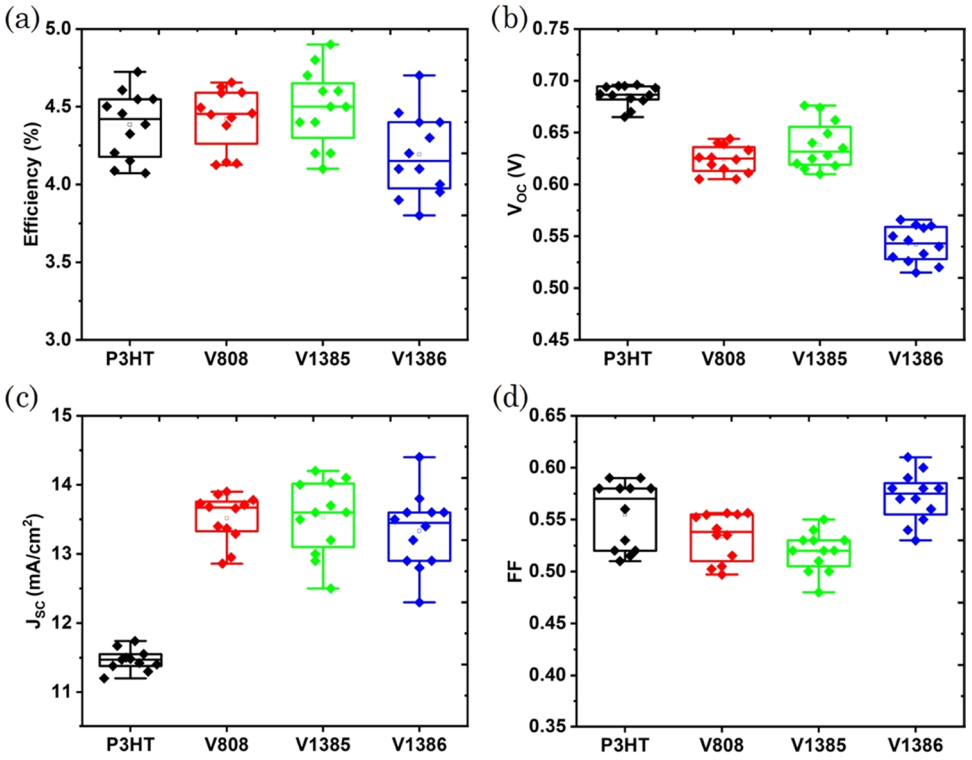

Figure 5. Reproducibility box plots of Sb_2S_3 solar cells with P3HT, **V808**, **V1385**, and **V1386** as HTMs: (a) Efficiency, (b) V_{OC}, (c) J_{SC}, and (d) fill factor (FF).

better wettability of new HTMs on the Sb_2S_3 surface. Therefore, despite possessing better interaction capability and favorable band edge positions, the solar cells with new HTMs have either marginally achieved similar V_{OC} as that of the conventional P3HT or have yielded lower values. In addition, it is known that mobility plays a crucial role in the performance of solar cells, but in this study, other factors that influence the PV parameters might be dominant. One of the important PV parameters is V_{OC} and its variation is generally ascribed to the energy levels, however, as they are quite similar, the other main aspect could be the interfacial recombination at Sb_2S_3-HTM. Now, there might be two sources of recombination—one is direct contact between the electrode and absorber layer (microshunts), due to the thinner films (which could explain lower V_{OC} than P3HT), second—the quality of the interface between the absorber and HTM. Thiophenes, in principle, are introduced for the better interface, for e.g., surface passivation, however, then one would expect the best performance for **V1386**. So, a further inspection of the Sb_2S_3-HTM interface through advanced characterization techniques like deep-level transient spectroscopy may be needed to understand the role of interfacial defects on the performance of solar cells, and can be explored in future studies.

The cross-sectional images of solar cells with P3HT and new HTMs are shown in Figure 4c. While TiO_2 and Sb_2S_3 have an almost similar thickness in each case, P3HT is reasonably thicker (≈100 nm) compared to the new HTMs (≈25−30 nm). It may be noted that each individual HTM herein is optimized by its precursor concentration in spin coating to obtain the best efficient solar cells. Apparently, a thick P3HT is needed in order to get an efficiency of ≈4.7% whereas a considerably thinner layer of each of the new HTMs is sufficient to obtain similar or slightly higher efficiencies (4.5−4.9%). This proves the fact that the new HTMs, particularly **V808** and **V1385**, are not only considerably cheaper but also the required materials consumption is significantly lower, which warrants the plausible fabrication of Sb_2S_3 solar cells with efficiencies close to 5% at a much cheaper cost. In addition, for the reproducibility of devices, the statistical box plots of efficiency, and the associated device parameters are shown in Figure 5. As Figure 5a unveils, the efficiency spread is almost identical in each case with P3HT and new HTMs. Further, the average efficiencies are also in a similar range in each of the optimized cases, except for the case of **V1386**, which shows a slightly lower efficiency owing to the low V_{OC}. Similarly, the trend in V_{OC}, J_{SC}, and FF is almost the same as that for the champion numbers with reasonably identical spreads. The V_{OC} in **V1386**-based solar cells is considerably lower while the J_{SC} in P3HT-solar cells is the lowest and the FFs range from 0.5 to 0.6 in all the cases. As the statistics indicate, the high reproducibility of the results is obtained in the present study.

The normalized external quantum efficiency (EQE) curves of solar cells with P3HT and new HTM layers are shown in Figure 6a. In addition, the integrated photocurrent density ($J_{integrated}$) calculated using EQE spectra is also shown and it can be noted that almost identical J_{SC} values are obtained from EQE data to the values extracted from $J-V$ curves. A pertinent aspect to be noted is the dip in EQE for solar cells with P3HT in the range of 500−650 nm, which may be attributed to the parasitic absorption losses.[2] When an absorber is thinner or comparable to the thickness of HTM, the light that gets transmitted through the absorber gets reflected back from the back contact and often, the reflected light could be reabsorbed in the absorber to result in photogenerated carriers. However, if the HTM is sufficiently thick, then the reflected light gets

https://doi.org/10.1021/acsaem.2c04097
ACS Appl. Energy Mater. 2023, 6, 3822−3833

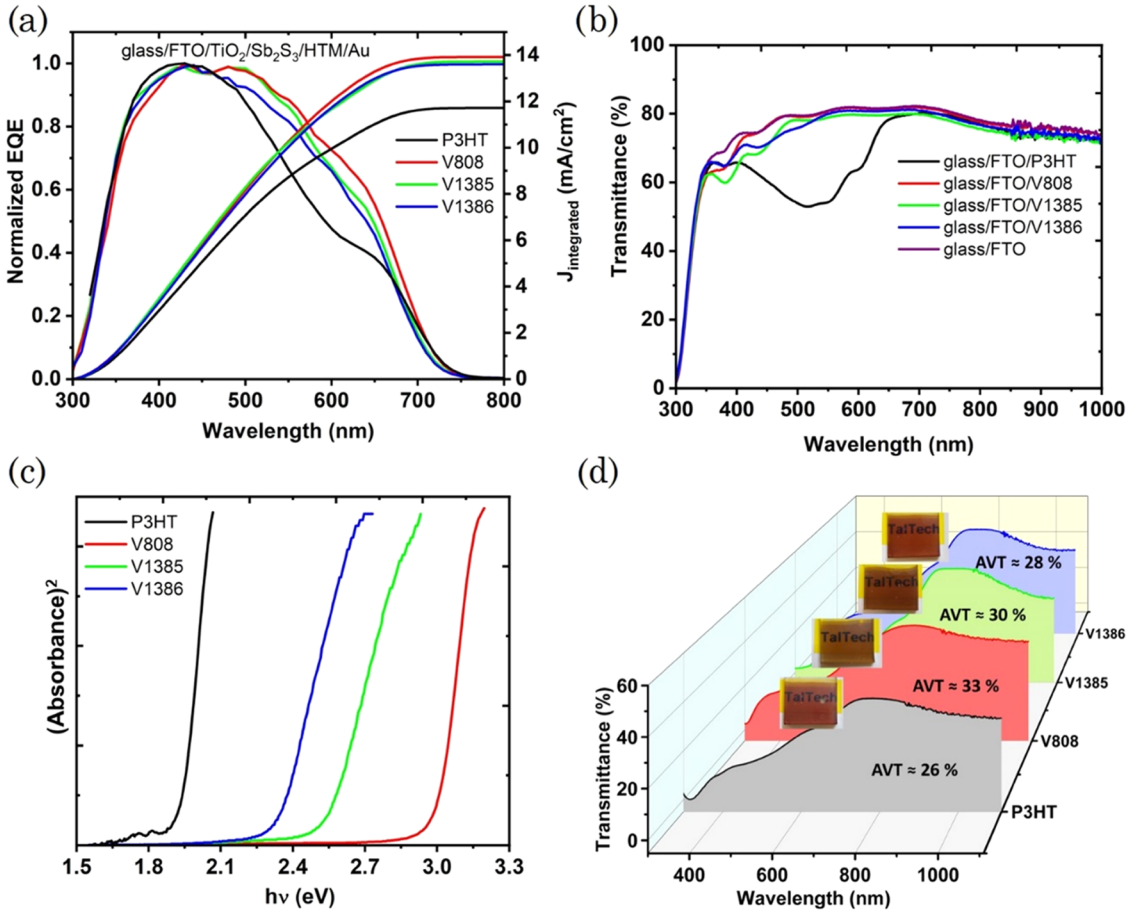

Figure 6. (a) Normalized external quantum efficiency (EQE) curves and the integrated J_{SC} of Sb_2S_3 solar cells with P3HT, **V808**, **V1385**, and **V1386** as HTMs, (b) transmittance curves of glass/FTO, glass/FTO/P3HT, glass/FTO/**V808**, glass/FTO/**V1385** and glass/FTO/**V1386**, (c) $(absorbance)^2$ vs $h\nu$ plots of P3HT, **V808**, **V1385**, and **V1386** for band gap determination, and (d) transmittance curves of the device stack with P3HT, **V808**, **V1385**, and **V1386** as HTMs without Au (inset: Respective sample photographs captured with a background showing semi-transparency).

absorbed in the HTM layer leading to parasitic absorption. In this study, P3HT is considerably thick and thus exhibits parasitic absorption while the considerably thinner new HTMS (**V808**, **V1385**, and **V1386**) does not show any similar dip in EQE, which could further explain the enhanced J_{SC} values in the respective solar cells. Optical transmittance studies are performed for bare P3HT and new **V808**, **V1385**, and **V1386** HTM layers on glass/FTO substrates, as shown in Figure 6b, where the absorption by P3HT is corroborated with EQE results as observed from the dip in transmittance in 400−650 nm region. Further, it may also be observed that the new HTMs exhibit considerable transparency similar to that of the glass/FTO substrate. The band gaps of P3HT, **V808**, **V1385**, and **V1386** are inferred to be ≈1.9, 2.9, 2.5, and 2.3 eV, respectively, from the plots shown in Figure 6c and the absorption coefficient-based Tauc's plots in Figure S4, which ascertains the fact that new HTMs are optically more transparent in the visible region compared to P3HT. Finally, the overall transparency of device stacks without top metal contact is analyzed (see Figure 6d) and the solar weighted average visible transmittance (AVT) (400−800 nm) of devices with P3HT, **V808**, **V1385**, and **V1386** HTMs are determined to be ≈26, 33, 30, and 28%, respectively. In the case of new HTMs, as the thiophene units increased the band gap decreased resulting in slightly reduced transparency as witnessed from the overall device transmittance. The sample pictures of glass/FTO/TiO_2/Sb_2S_3/HTM where HTM is P3HT, **V808**, **V1385**, and **V1386** are shown with a background and it may be observed that all the samples exhibit decent transparency with visibility being the highest for **V808**. While all device stacks exhibit reasonably good AVT values as required for semitransparent applications, the devices with new HTMs exhibit enhanced transparency, which is due to their increased transmittance over P3HT. The cost-effective fluorene-based thiophene-terminated (**V808**, **V1385**, **V1386**) HTMs are successfully demonstrated in Sb_2S_3 solar cells as potentially suitable candidates for semitransparent applications and efforts are underway to increase the PCE of solar cells and upscaling the devices.

4. CONCLUSIONS

Novel cost-effective and transparent fluorene-based thiophene-terminated hole transport materials (**V808**, **V1385**, and **V1386**) are demonstrated, for the first time, in semitransparent Sb_2S_3 solar cells exhibiting a power conversion efficiency of 4.5−4.9% and an average visible transmittance of 30−33% (without the metal) in the 400−800 nm range. Solar cells with the conventional P3HT as HTM have yielded 4.7% efficiency, however, they have exhibited lower transparency (26%) owing to parasitic absorption losses in P3HT. The band diagram of

https://doi.org/10.1021/acsaem.2c04097
ACS Appl. Energy Mater. 2023, 6, 3822−3833

solar cells with new HTMs and P3HT are compared, which unveils that new HTMs have exhibited favorable band offset validating them as effective HTMs for Sb_2S_3 solar cells. The new HTMs with terminated thiophene units have demonstrated reasonably improved wettability over conventional P3HT that could provide better interaction channels for charge carrier transport thus leading to enhanced current density. However, a closer inspection of Sb_2S_3-HTM needs to be further explored to unravel the interfacial effects as the solar cells with new HTMs have exhibited reasonably lower V_{OC} values, particularly in the case of **V808** and **V1386**.

■ ASSOCIATED CONTENT

Supporting Information

The Supporting Information is available free of charge at https://pubs.acs.org/doi/10.1021/acsaem.2c04097.

Synthesis procedure, DSC, $J-V$ characteristics of solar cells, and absorption spectra related data of **V808**, **V1385**, and **V1386** (PDF)

■ AUTHOR INFORMATION

Corresponding Authors

Sreekanth Mandati − *Department of Materials and Environmental Technology, Laboratory of Thin Film Chemical Technologies, Tallinn University of Technology, 19086 Tallinn, Estonia;* orcid.org/0000-0002-3317-271X; Email: sreekanth.mandati@taltech.ee

Ilona Oja Acik − *Department of Materials and Environmental Technology, Laboratory of Thin Film Chemical Technologies, Tallinn University of Technology, 19086 Tallinn, Estonia*; Email: ilona.oja@taltech.ee

Authors

Nimish Juneja − *Department of Materials and Environmental Technology, Laboratory of Thin Film Chemical Technologies, Tallinn University of Technology, 19086 Tallinn, Estonia*

Atanas Katerski − *Department of Materials and Environmental Technology, Laboratory of Thin Film Chemical Technologies, Tallinn University of Technology, 19086 Tallinn, Estonia*

Aistė Jegorovė − *Department of Organic Chemistry, Kaunas University of Technology, Kaunas LT-50254, Lithuania*

Raitis Grzibovskis − *Institute of Solid State Physics, University of Latvia, Riga LV 1063, Latvia*

Aivars Vembris − *Institute of Solid State Physics, University of Latvia, Riga LV 1063, Latvia*

Tatjana Dedova − *Department of Materials and Environmental Technology, Laboratory of Thin Film Chemical Technologies, Tallinn University of Technology, 19086 Tallinn, Estonia*

Nicolae Spalatu − *Department of Materials and Environmental Technology, Laboratory of Thin Film Chemical Technologies, Tallinn University of Technology, 19086 Tallinn, Estonia;* orcid.org/0000-0003-0234-2170

Artiom Magomedov − *Department of Organic Chemistry, Kaunas University of Technology, Kaunas LT-50254, Lithuania;* orcid.org/0000-0003-3159-1870

Smagul Karazhanov − *Institute for Energy Technology (IFE), NO 2027 Kjeller, Norway*

Vytautas Getautis − *Department of Organic Chemistry, Kaunas University of Technology, Kaunas LT-50254, Lithuania;* orcid.org/0000-0001-7695-4677

Malle Krunks − *Department of Materials and Environmental Technology, Laboratory of Thin Film Chemical Technologies, Tallinn University of Technology, 19086 Tallinn, Estonia;* orcid.org/0000-0003-4658-4403

Complete contact information is available at: https://pubs.acs.org/10.1021/acsaem.2c04097

Author Contributions

S.M. conceptualization, design of experiments, analysis of the results, and manuscript writing; N.J. experiments and contribution to manuscript writing; A.K. and T.D. support in experiments and data acquisition; N.S. and S.K. supported in analysis; A.J., A.M., and V.G. synthesized and characterized new HTMs; R.G. and A.V. performed ionization potential and hole mobility measurements, M.K. and I.O.A. provided support for analysis and finalizing the manuscript draft. All authors have given approval to the final version of the manuscript.

Funding

EEA Grants—S-BMT-21-1(LT08-2-LMT-K-01-003). Estonian Research Council—PRG627 and PSG689. Archimedes Foundation—TK141 (TAR16016EK). European Union Horizon2020—952509 and 739508.

Notes

The authors declare no competing financial interest.

■ ACKNOWLEDGMENTS

The "Development of Semitransparent Bifacial Thin-Film Solar Cells for Innovative Applications" benefits from a 999372 € grant from Iceland, Liechtenstein, and Norway through the EEA Grants. The aim of the project is to develop a new approach based on novel materials and structures and production technologies, which are the key to further increase the share and range of applications of PV in areas with sub-average sunlight, including Baltic and Nordic countries. Therefore, the development of resource saving, cost-effective, and efficient PV devices is a primary challenge of this project. Project contract with the Research Council of Lithuania (LMTLT) number is S-BMT-21-1(LT08-2-LMT-K-01-003). Department of Materials and Environmental Technology, Tallinn University of Technology has received funding from the Estonian Research Council projects PRG627 "Antimony chalcogenide thin films for next-generation semitransparent solar cells applicable in electricity producing windows" and PSG689 "Bismuth Chalcogenide Thin-Film Disruptive Green Solar Technology for Next-Generation Photovoltaics", and the Estonian Centre of Excellence project TK141 (TAR16016EK) "Advanced materials and high-technology devices for energy recuperation systems", the European Union's Horizon2020 program under the ERA Chair project 5GSOLAR grant agreement No 952509. Institute of Solid-State Physics, University of Latvia has received funding from the European Union's Horizon2020 Framework Programme H2020-WIDESPREAD-01-2016-2017-TeamingPhase2 under grant agreement no. 739508, project CAMART^2. The authors thank Dr. Tadas Malinauskas and Dr. Valdek Mikli for their support in the preparation and characterization of the samples.

ABBREVIATIONS

HTM, hole transport material
V808, N^2,N^2,N^7,N^7-tetrakis(4-methoxyphenyl)-9-(thiophen-2-ylmethylene)-9*H*-fluorene-2,7-diamine
V1385, 9-([2,2′:5′,2″-terthiophen]-5-ylmethylene)-N^2,N^2,N^7,N^7-tetrakis(4-methoxyphenyl)-9*H*-fluorene-2,7-diamine
V1386, 9-([2,2′-bithiophen]-5-ylmethylene)-N^2,N^2,N^7,N^7-tetrakis(4-methoxyphenyl)-9*H*-fluorene-2,7-diamine
P3HT, poly(3-hexylthiophene)
Spiro-OMeTAD, 2,2′,7,7′-tetrakis[*N*,*N*-di(4-methoxyphenyl)amino]-9,9′-spirobifluorene
PCPDTBT, poly{4,4-dialkyl-4*H*-cyclopenta[2,1-*b*;3,4-*b*′]-dithiophene-2,6-diyl-*alt*-2,1,3-benzothiadiazole-4,7-diyl}
AVT, average visible transmittance
DSC, differential scanning calorimetry
TGA, thermal gravimetric analysis
EQE, external quantum efficiency

REFERENCES

(1) Kondrotas, R.; Chen, C.; Tang, J. Sb2S3 Solar Cells. *Joule* **2018**, *2*, 857−878.
(2) Zimmermann, E.; Pfadler, T.; Kalb, J.; Dorman, J. A.; Sommer, D.; Hahn, G.; Weickert, J.; Schmidt-Mende, L. Toward High-Efficiency Solution-Processed Planar Heterojunction Sb2S3 Solar Cells. *Adv. Sci.* **2015**, *2*, No. 1500059.
(3) Castro, J. R.; Dale, P.; Mahon, M. F.; Molloy, K. C.; Peter, L. M. Deposition of Antimony Sulfide Thin Films from Single-Source Antimony Thiolate Precursors. *Chem. Mater.* **2007**, *19*, 3219−3226.
(4) Büttner, P.; Scheler, F.; Döhler, D.; Barr, M. K. S.; Bosch, M.; Rey, M.; Yokosawa, T.; Hinz, S.; Maultzsch, J.; Spiecker, E.; Vogel, N.; Mínguez-Bacho, I.; Bachmann, J. Continuous, Crystalline Sb2S3 Ultrathin Light Absorber Coatings in Solar Cells Based on Photonic Concentric p-i-n Heterojunctions. *Nano Energy* **2022**, *103*, No. 107820.
(5) Shah, U. A.; Chen, S.; Khalaf, G. M. G.; Jin, Z.; Song, H. Wide Bandgap Sb2S3 Solar Cells. *Adv. Funct. Mater.* **2021**, *31*, No. 2100265.
(6) Eensalu, J. S.; Katerski, A.; Kärber, E.; Weinhardt, L.; Blum, M.; Heske, C.; Yang, W.; Acik, I. O.; Krunks, M. Semitransparent Sb2S3 Thin Film Solar Cells by Ultrasonic Spray Pyrolysis for Use in Solar Windows. *Beilstein J. Nanotechnol.* **2019**, *10*, 2396−2409.
(7) Lee, S.-J.; Sung, S.-J.; Yang, K.-J.; Kang, J.-K.; Kim, J. Y.; Do, Y. S.; Kim, D.-H. Approach to Transparent Photovoltaics Based on Wide Band Gap Sb2S3 Absorber Layers and Optics-Based Device Optimization. *ACS Appl. Energy Mater.* **2020**, *3*, 12644−12651.
(8) Wang, S.; Zhao, Y.; Che, B.; Li, C.; Chen, X.; Tang, R.; Gong, J.; Wang, X.; Chen, G.; Chen, T.; Li, J.; Xiao, X. A Novel Multi-Sulfur Source Collaborative Chemical Bath Deposition Technology Enables 8%-Efficiency Sb2S3 Planar Solar Cells. *Adv. Mater.* **2022**, *34*, No. 2206242.
(9) Yang, Z.; Wang, X.; Chen, Y.; Zheng, Z.; Chen, Z.; Xu, W.; Liu, W.; Yang Michael, Y.; Zhao, J.; Chen, T.; Zhu, H. Ultrafast Self-Trapping of Photoexcited Carriers Sets the Upper Limit on Antimony Trisulfide Photovoltaic Devices. *Nat. Commun.* **2019**, *10*, No. 4540.
(10) Dong, J.; Liu, Y.; Wang, Z.; Zhang, Y. Boosting VOC of Antimony Chalcogenide Solar Cells: A Review on Interfaces and Defects. *Nano Sel.* **2021**, *2*, 1818−1848.
(11) Krautmann, R.; Spalatu, N.; Gunder, R.; Abou-Ras, D.; Unold, T.; Schorr, S.; Krunks, M.; Oja Acik, I. Analysis of Grain Orientation and Defects in Sb2Se3 Solar Cells Fabricated by Close-Spaced Sublimation. *Sol. Energy* **2021**, *225*, 494−500.
(12) Vidal-Fuentes, P.; Placidi, M.; Sánchez, Y.; Becerril-Romero, I.; Andrade-Arvizu, J.; Jehl, Z.; Pérez-Rodríguez, A.; Izquierdo-Roca, V.; Saucedo, E. Efficient Se-Rich Sb2Se3/CdS Planar Heterojunction Solar Cells by Sequential Processing: Control and Influence of Se Content. *Sol. RRL* **2020**, *4*, No. 2000141.
(13) Hobson, T. D. C.; Phillips, L. J.; Hutter, O. S.; Shiel, H.; Swallow, J. E. N.; Savory, C. N.; Nayak, P. K.; Mariotti, S.; Das, B.; Bowen, L.; Jones, L. A. H.; Featherstone, T. J.; Smiles, M. J.; Farnworth, M. A.; Zoppi, G.; Thakur, P. K.; Lee, T.-L.; Snaith, H. J.; Leighton, C.; Scanlon, D. O.; Dhanak, V. R.; Durose, K.; Veal, T. D.; Major, J. D. Isotype Heterojunction Solar Cells Using N-Type Sb2Se3 Thin Films. *Chem. Mater.* **2020**, *32*, 2621−2630.
(14) Zhu, L.; Chen, J.; Liu, R.; Dong, C.; Yang, S.; Chen, T.; Chen, C.; Qiao, Q.; Wang, M. Solution-Processed Compact Sb2S3 Thin Films by a Facile One-Step Deposition Method for Efficient Solar Cells. *Sol. RRL* **2021**, *5*, No. 2100666.
(15) Choi, Y. C.; Lee, D. U.; Noh, J. H.; Kim, E. K.; Seok, S. Il. Highly Improved Sb2S3 Sensitized-Inorganic−Organic Heterojunction Solar Cells and Quantification of Traps by Deep-Level Transient Spectroscopy. *Adv. Funct. Mater.* **2014**, *24*, 3587−3592.
(16) You, M. S.; Lim, C.-S.; Kwon, D. H.; Heo, J. H.; Im, S. H.; Chae, K. J. Oxide-Free Sb2S3 Sensitized Solar Cells Fabricated by Spin and Heat-Treatment of Sb(III)(Thioacetamide)2Cl3. *Org. Electron.* **2015**, *21*, 155−159.
(17) Zhang, Y.; Li, S.; Tang, R.; Wang, X.; Chen, C.; Lian, W.; Zhu, C.; Chen, T. Phosphotungstic Acid Regulated Chemical Bath Deposition of Sb2S3 for High-Efficiency Planar Heterojunction Solar Cell. *Energy Technol.* **2018**, *6*, 2126−2131.
(18) Chen, J.; Qi, J.; Liu, R.; Zhu, X.; Wan, Z.; Zhao, Q.; Tao, S.; Dong, C.; Ashebir, G. Y.; Chen, W.; Peng, R.; Zhang, F.; Yang, S.; Tian, X.; Wang, M. Preferentially Oriented Large Antimony Trisulfide Single-Crystalline Cuboids Grown on Polycrystalline Titania Film for Solar Cells. *Commun. Chem.* **2019**, *2*, No. 121.
(19) Nie, R.; Seok, S. Il. Efficient Antimony-Based Solar Cells by Enhanced Charge Transfer. *Small Methods* **2020**, *4*, No. 1900698.
(20) Nie, R.; Yun, H.; Paik, M.-J.; Mehta, A.; Park, B.; Choi, Y. C.; Seok, S. Il. Efficient Solar Cells Based on Light-Harvesting Antimony Sulfoiodide. *Adv. Energy Mater.* **2018**, *8*, No. 1701901.
(21) Liu, C. P.; Wang, H. E.; Ng, T. W.; Chen, Z. H.; Zhang, W. F.; Yan, C.; Tang, Y. B.; Bello, I.; Martinu, L.; Zhang, W. J.; Jha, S. K. Hybrid Photovoltaic Cells Based on ZnO/Sb2S3/P3HT Heterojunctions. *Phys. Status Solidi B* **2012**, *249*, 627−633.
(22) Reeja-Jayan, B.; Manthiram, A. Effects of Bifunctional Metal Sulfide Interlayers on Photovoltaic Properties of Organic−Inorganic Hybrid Solar Cells. *RSC Adv.* **2013**, *3*, 5412−5421.
(23) Kärber, E.; Katerski, A.; Acik, I. O.; Mere, A.; Mikli, V.; Krunks, M. Sb2S3 Grown by Ultrasonic Spray Pyrolysis and Its Application in a Hybrid Solar Cell. *Beilstein J. Nanotechnol.* **2016**, *7*, 1662−1673.
(24) Wang, X.; Li, J.; Liu, W.; Yang, S.; Zhu, C.; Chen, T. A Fast Chemical Approach towards Sb2S3 Film with a Large Grain Size for High-Performance Planar Heterojunction Solar Cells. *Nanoscale* **2017**, *9*, 3386−3390.
(25) Lan, C.; Liang, G.; Lan, H.; Peng, H.; Su, Z.; Zhang, D.; Sun, H.; Luo, J.; Fan, P. Microstructural and Optical Properties of Sb2S3 Film Thermally Evaporated from Antimony Pentasulfide and Efficient Planar Solar Cells. *Phys. Status Solidi RRL* **2018**, *12*, No. 1800025.
(26) Han, J.; Pu, X.; Zhou, H.; Cao, Q.; Wang, S.; He, Z.; Gao, B.; Li, T.; Zhao, J.; Li, X. Synergistic Effect through the Introduction of Inorganic Zinc Halides at the Interface of TiO2 and Sb2S3 for High-Performance Sb2S3 Planar Thin-Film Solar Cells. *ACS Appl. Mater. Interfaces* **2020**, *12*, 44297−44306.
(27) Han, J.; Wang, S.; Yang, J.; Guo, S.; Cao, Q.; Tang, H.; Pu, X.; Gao, B.; Li, X. Solution-Processed Sb2S3 Planar Thin Film Solar Cells with a Conversion Efficiency of 6.9% at an Open Circuit Voltage of 0.7 V Achieved via Surface Passivation by a SbCl3 Interface Layer. *ACS Appl. Mater. Interfaces* **2020**, *12*, 4970−4979.
(28) Tang, R.; Wang, X.; Lian, W.; Huang, J.; Wei, Q.; Huang, M.; Yin, Y.; Jiang, C.; Yang, S.; Xing, G.; Chen, S.; Zhu, C.; Hao, X.; Green, M. A.; Chen, T. Hydrothermal Deposition of Antimony Selenosulfide Thin Films Enables Solar Cells with 10% Efficiency. *Nat. Energy* **2020**, *5*, 587−595.
(29) Lian, W.; Jiang, C.; Yin, Y.; Tang, R.; Li, G.; Zhang, L.; Che, B.; Chen, T. Revealing Composition and Structure Dependent Deep-

https://doi.org/10.1021/acsaem.2c04097
ACS Appl. Energy Mater. 2023, 6, 3822−3833

Level Defect in Antimony Trisulfide Photovoltaics. *Nat. Commun.* **2021**, *12*, No. 3260.
(30) Ning, H.; Guo, H.; Zhang, J.; Wang, X.; Jia, X.; Qiu, J.; Yuan, N.; Ding, J. Enhancing the Efficiency of Sb2S3 Solar Cells Using Dual-Functional Potassium Doping. *Sol. Energy Mater. Sol. Cells* **2021**, *221*, No. 110816.
(31) Büttner, P.; Scheler, F.; Pointer, C.; Döhler, D.; Yokosawa, T.; Spiecker, E.; Boix, P. P.; Young, E. R.; Mínguez-Bacho, I.; Bachmann, J. ZnS Ultrathin Interfacial Layers for Optimizing Carrier Management in Sb2S3-Based Photovoltaics. *ACS Appl. Mater. Interfaces* **2021**, *13*, 11861−11868.
(32) Kim, D.-H.; Lee, S.-J.; Park, M. S.; Kang, J.-K.; Heo, J. H.; Im, S. H.; Sung, S.-J. Highly Reproducible Planar Sb2S3-Sensitized Solar Cells Based on Atomic Layer Deposition. *Nanoscale* **2014**, *6*, 14549−14554.
(33) Juneja, N.; Mandati, S.; Katerski, A.; Spalatu, N.; Daskeviciute-Geguziene, S.; Vembris, A.; Karazhanov, S.; Getautis, V.; Krunks, M.; Oja Acik, I. Sb2S3 Solar Cells with a Cost-Effective and Dopant-Free Fluorene-Based Enamine as a Hole Transport Material. *Sustainable Energy Fuels* **2022**, *6*, 3220−3229.
(34) Petrus, M. L.; Bein, T.; Dingemans, T. J.; Docampo, P. A Low Cost Azomethine-Based Hole Transporting Material for Perovskite Photovoltaics. *J. Mater. Chem. A* **2015**, *3*, 12159−12162.
(35) Eensalu, J. S.; Katerski, A.; Kärber, E.; Acik, I. O.; Mere, A.; Krunks, M. Uniform Sb2S3 Optical Coatings by Chemical Spray Method. *Beilstein J. Nanotechnol.* **2019**, *10*, 198−210.
(36) Jiang, C.; Zhou, J.; Tang, R.; Lian, W.; Wang, X.; Lei, X.; Zeng, H.; Zhu, C.; Tang, W.; Chen, T. 9.7%-Efficient Sb2(S,Se)3 Solar Cells with a Dithieno[3,2-b: 2′,3′-d]Pyrrole-Cored Hole Transporting Material. *Energy Environ. Sci.* **2021**, *14*, 359−364.
(37) Xiang, Y.; Guo, H.; Cai, Z.; Jiang, C.; Zhu, C.; Wu, Y.; Zhu, W.-H.; Chen, T. Dopant-Free Hole-Transporting Materials for Stable Sb2(S,Se)3 Solar Cells. *Chem. Commun.* **2022**, *58*, 4787−4790.

https://doi.org/10.1021/acsaem.2c04097
ACS Appl. Energy Mater. 2023, 6, 3822−3833